Revista Mexicana de Astronomía y Astrofísica, **33**, 165–171 (1997)

PHOTODISSOCIATED H I IN NGC 2023

M. Lebrón and L. F. Rodríguez

Instituto de Astronomía
Universidad Nacional Autónoma de México

Received 1997 June 20; accepted 1997 September 3

RESUMEN

Reportamos la detección de H I fotodisociado alrededor de la nebulosa de reflexión NGC 2023. Las observaciones realizadas con el Conjunto Muy Grande de Radiotelescopios (Very Large Array) revelan emisión compacta ($\sim$ 0.3 pc) asociada a la fuente. El espectro observado tiene un perfil de doble pico, el cual interpretamos como producido por absorción debida a gas neutro que se encuentra entre la región H I compacta y el observador. El espectro fue corregido por esta absorción y con el espectro corregido determinamos una densidad columnar y una masa de H I de 1.7×10^{21} cm^{-2} y 1.2 $M_{\odot}$, respectivamente. Esta densidad columnar es consistente con predicciones de modelos teóricos. El mapa de H I a 21 cm muestra una morfología muy similar a la que se observa en los mapas de [C II] a 158 μm, HIRES de *IRAS* a 60 μm y el mapa óptico del POSS.

ABSTRACT

We report the detection of photodissociated H I toward the reflection nebula NGC 2023. The Very Large Array observations reveal compact ($\sim$ 0.3 pc) emission associated with the source. The observed spectrum has a double-peaked profile that we believe is caused by absorbing foreground neutral gas. We corrected the observed spectrum for the absorption, and determined with this absorption-corrected profile an H I column density and mass of 1.7×10^{21} cm^{-2} and 1.2 $M_{\odot}$, respectively. This column density agrees well with theoretical model predictions. The H I 21 cm map shows a morphology very similar to that present in the images of [C II] at 158 μm, HIRES 60 μm *IRAS*, and POSS optical.

Key words: **ISM – ATOMS — ISM – INDIVIDUAL (NGC 2023) — ISM – REFLECTION NEBULAE — RADIO LINES – INTERSTELLAR**

1. INTRODUCTION

Young luminous stars embedded in molecular clouds are expected to photodissociate molecular hydrogen, producing an H I zone. If the star is hot enough, an inner H II region can also be produced. Recent studies of photodissociated H I regions include SVS 3 (Rodríguez et al. 1990), IRAS 23545+6508 (Dewdney et al. 1991), Sh 217 and Sh 219 (Roger & Leahy 1993), NGC 7023 (Rogers, Heyer, & Dewdney 1995), and IC 1396 (Moriarty-Schieven, Xie, & Patel 1996).

In principle, the mass and size of an H I region can be used to determine the spectral type of the photodissociating star (e.g., Rodríguez et al. 1990), potentially providing an important tool for the study of embedded stars. However, observations of galactic H I are difficult, and severely limited by the presence of large amounts of extended atomic gas along almost every line-of-sight in the galactic plane. In only a handful of sources it has been possible to detect photodissociated H I unambiguously.

To search for new photodissociated regions in association with intermediate mass stars, we undertook a VLA program of H I observations toward seven candidate sources (see Table 1). In two of these, NGC 2023 and GGD 12–15, we clearly detected compact ($\sim$ 0.1–0.3 pc) H I associated with the source. The GGD 12–15 results are discussed in Gómez et al. 1997; here we report the results for NGC 2023.

NGC 2023 is a reflection nebula in the L1630 molecular cloud, about 20′ south of the H II region NGC 2024 (Orion B). Its distance is 450–500 pc,

TABLE 1

OBSERVED REGIONS

Name	Phase Center α (1950)	δ (1950)	V_{LSR} (km s^{-1})	Velocity Range with Extended H I (km s^{-1})	Phase Calibrator	Bootstrapped Flux Density (Jy)
NGC 1435	$03^h43^m12.0^s$	23°37′00″	−10.00	−13.9 to 20.9	0400 + 258	0.927 ± 0.004
NGC 1999	05 34 06.0	−06 44 00	9.00	−16.8 to 36.1	0539 − 057	0.865 ± 0.004
NGC 2023	05 39 12.0	−02 14 00	9.00	15.4 to 19.2	0539 − 057	0.865 ± 0.004
GGD 12–15	06 08 24.0	−06 11 00	9.00	0.0 to 10.3	0605 − 085	2.165 ± 0.011
NGC 2261	06 36 24.0	08 46 00	9.00	−14.2 to 39.9	0629 + 104	1.568 ± 0.012
NGC 7129	21 40 06.0	65 42 00	−10.00	−78.3 to 10.6	2201 + 624	2.130 ± 0.017
Cep A	22 54 20.0	61 46 00	−10.00	−91.2 to 28.7	2348 + 643	3.238 ± 0.027

and it is illuminated by the B1.5 V star HD 37903. The optical nebulosity extends about 10′ around the central star. Radio continuum emission has been reported at 6 cm ($S_\nu \sim 32$ mJy beam^{-1}) near HD 37903 (Pankonin & Walmsley 1976), the exciting star of NGC 2023. Several near-infrared (NIR) sources were found embedded in the nebulosity (Sellgren 1983; Sellgren, Werner, & Dinerstein 1992), and dense cores were detected in CS (Lada, Bally, & Stark 1991; Launhardt et al. 1996). The region also contains the emission line star Lk-Hα 287. All these data together, indicate that NGC 2023 is a region of recent star formation. The reflection nebula is also associated with photodissociated gas, evident through a C$^+$ region generated by the dissociation of CO followed by the immediate ionization of the C I by the far ultraviolet radiation of HD 37903 (Knapp, Brown, & Kuiper 1975). The C$^+$ region has been detected in the forbidden line of [C II] at 158 μm (Howe et al. 1991; Jaffe et al. 1990; Crawford et al. 1985; Steiman-Cameron et al. 1997) and in carbon radio recombination lines (Knapp et al. 1975; Pankonin & Walmsley 1976, 1978; Wyrowski et al. 1997). In this work we present the detection of the 21 cm H I line toward NGC 2023 and discuss its relationship with the C$^+$ region, the far-infrared (FIR) dust emission and the molecular cloud.

2. OBSERVATIONS

Observations of the 21 cm line of H I (ν_o = 1.420405752 GHz) were made using the VLA interferometer of the NRAO[1] during 1991 March 25, 26 and 29. The array was in its most compact (D) configuration, giving a typical synthesized beam of ∼ 50″ with uniform weighting. For all observations, a total bandwidth of 0.781 MHz (128 channels of 6.103 kHz = 1.288 km s^{-1} each) was employed. Typical on-source integration times were one hour, and both circular polarizations were observed. The data were edited and calibrated using the software package AIPS of NRAO. The absolute amplitude and bandpass calibrator was 0134+329 with an adopted flux density of 16.05 Jy. The observed sources and their corresponding phase calibrators (with their bootstrapped flux densities) are given in Table 1.

Extended H I (present on scales comparable to the ∼ 30′ primary beam) was detected in all cases, and the velocity extent of this emission is given in Table 1. We attribute this extended emission to line-of-sight H I in diffuse clouds. As noted above, compact (< 3′) H I in emission was detected clearly toward GGD 12–15 and NGC 2023. In the following we discuss our results for NGC 2023.

3. RESULTS AND DISCUSSION

3.1. The Spatial Distribution of H I Emission

Figure 1 shows ten channel maps spanning the range of compact H I emission around NGC 2023. Only channels with compact 21 cm emission associated with the source are shown. The emission is roughly centered on the position of HD 37903, but clearly shows varying structure with velocity. The emission to the southeast of the star is present throughout the entire velocity range, with a minimum at 10.3 km s^{-1} (approximately equal to the LSR velocity of NGC 2023). We note that between 12.9 and 11.6 km s^{-1}, there is emission located ∼ 2′ to the north of the star. Also, between 14.2 and 12.9 km s^{-1} the 21 cm emission extends ∼ 2′ to the west of the star (1′ = 0.15 pc at a distance of 500 pc).

[1] The National Radio Astronomy Observatory is operated by Associated Universities Inc. under cooperative agreement with the National Science Foundation of the USA.

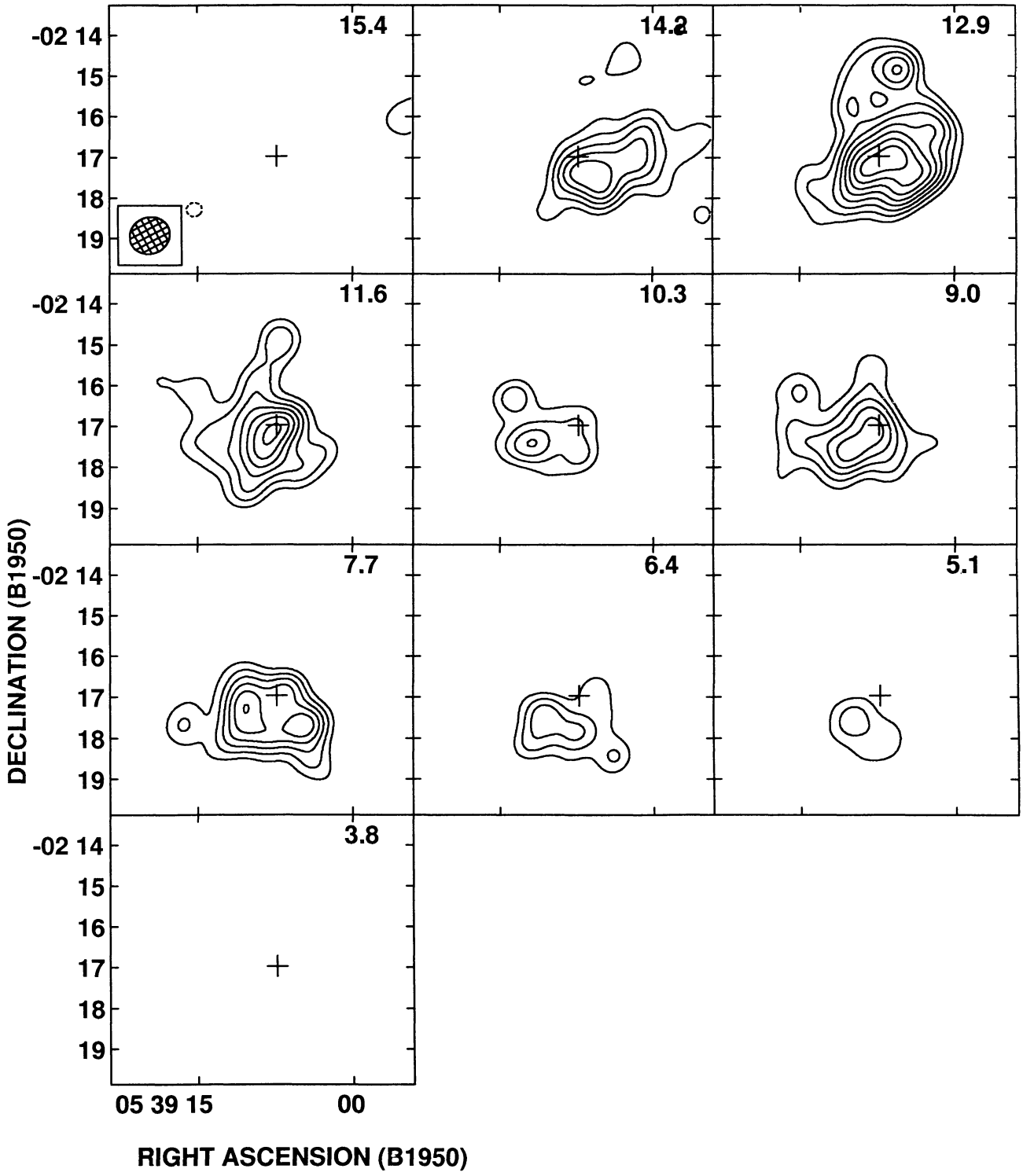

Fig. 1. Uniform-weight VLA maps of the H I 21 cm line emission toward NGC 2023. The central LSR velocity of each channel is shown in the top-right corner of each panel. The width of each channel is 1.288 km s^{-1}. Contours are −5, 5, 7, 9, 11, 13, 15, 17, 19 times 15 mJy $beam^{-1}$. The beam ($59'' \times 53''$; p.a.= $-61.^{\circ}9$) is shown in the first channel. The cross indicates the position of HD 37903 [$\alpha(1950) = 05^h39^m07.^s3$, $\delta(1950) = -02^o16'58''$].

3.2. The H I Spectrum

Figure 2 shows the line temperature as a function of velocity, averaged over an area of 2'.0×2'.7 around the position of HD 37903. The triangles represent the data points, that form a double-peaked spectrum. Two possible explanations for this double-peaked spectrum can be considered. First, two distinct velocity components may exist within the gas; and second, diffuse foreground H I may absorb part of the line emission. We discuss both possibilities in turn.

If we fit the spectrum with two Gaussian components (not shown), both components are shifted with respect to the cloud's LSR velocity of $\sim$ 10 km s^{-1}. The component velocity centers determined by the fit are 7.5 km s^{-1} (blueshifted) and 12.8 km s^{-1} (redshifted) with a full width half maximum (FWHM) of 4.0 and 2.9 km s^{-1}, respectively. If we assume the existence of these two velocity components in the H I gas, then it is reasonable to think that other material in the region may have a similar velocity distribution. However, CO (Kramer, Stutzki, & Winnewisser 1996), C92α (Wyrowski et al. 1997), and CS (Lada et al. 1991) line observations report only one velocity component in their emission, centered at $\sim$ 10 km s^{-1}. None of these observations show any evidence for two velocity components in the gas. We believe that the hypothesis of two velocity components is not a good explanation for the observed spectrum.

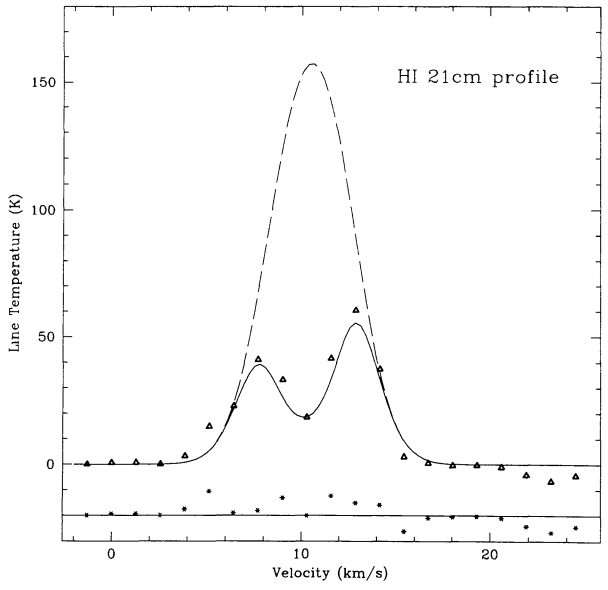

Fig 2. 21 cm spectrum averaged over a 2'.0 × 2'.7 field around HD 37903. Triangles are the data points, the continuous line is the best fit to the observed spectrum and the dashed curve is the fit after correction for foreground absorption. The residuals of the fit to the uncorrected spectrum are shown by the asterisks at the bottom of the figure. Table 2 lists the parameters derived from the fit.

We now consider the possibility that the line emission is absorbed by line-of-sight gas. If a diffuse medium lies between us and the source —a reasonable assumption given our present understanding of the ISM— we can obtain a simple approximation to the 21 cm line transport equation to predict the shape of the line for a plane-parallel geometry

$$T_L = (T_{ex} - T_{bg}) \times (1 - e^{-\tau_{HI}}) \times e^{-\tau_{dif}} \quad ; \quad (1)$$

where the opacity is given in general by

$$\tau = \tau_o exp \left[-4ln2 \left(\frac{v - v_o}{\Delta v} \right)^2 \right] ,$$

and T_{ex} is the excitation temperature of the 21 cm transition in the emitting region, T_{bg} is the cosmic background temperature (2.7 K), the subscripts $H\ I$ and dif refer to the emitting source (NGC 2023) and the diffuse absorbing medium respectively, τ_o is the opacity at the line center, v_o is the central velocity, and Δv is the FWHM of the line. Since the excitation temperature and the opacity are strongly correlated, they cannot be determined separately (Levinson & Brown 1980). We then adopted a value of 400 K for the excitation temperature of the emitting gas. This value is consistent with the range of gas temperatures determined by Steiman-Cameron et al. (1997) using IR lines of C II and O I. The continuous line in Figure 2 is the best fit considering an emitting region with a foreground H I absorbing medium (eq. 1). The parameters obtained from the fit are given in Table 2. We note that this absorbing medium could be line-of-sight H I or even the outer cooler parts of the cloud where NGC 2023 is embedded. We can estimate the "true" (unabsorbed) line profile of the source if the opacity of the diffuse medium (τ_{dif}) is now taken to be zero. The dashed line in Fig. 2, represents this absorption-corrected line profile.

Physical parameters of the H I emitting region can be calculated using both the observed (double peak) spectrum and the absorption-corrected (single peak) spectrum. We suppose that the H I line emission is optically thin to obtain a lower limit to the column density

$$N_{H\,I}(\mathrm{cm}^{-2}) = 1.822 \times 10^{18} \int \left(\frac{T_l}{K} \right) \left(\frac{dv}{\mathrm{km\ s}^{-1}} \right) . \quad (2)$$

Integrating the line over the observed spectrum (double peak profile), the H I column density is $N_{H\,I} \sim 6.5{\times}10^{20}$ cm^{-2}. We estimate the H I mass in the nebulosity using $\mathrm{M}_{H\,I} = m_H D^2 N_{H\,I} \Omega_s$, where D is the distance to the source, m_H is the mass of a hydrogen atom, $N_{H\,I}$ is the H I column den-

TABLE 2

FIT PARAMETERS OF THE 21 CM LINE OF H I

Component	v_o (km s^{-1})	Δv (km s^{-1})	τ_o
NGC 2023 H I (emission)	10.5	4.8	0.5
Diffuse foreground H I (absorption)	10.1	3.3	2.2

sity and Ω_s is the solid angle subtended by the source. The source size is estimated by the diameter of the half maximum contour from the map of integrated H I flux density (Figure 3). The estimated size is $\sim$ 2.'0 $\times$ 2.'7, and the resulting H I mass is $M_{HI} \sim 0.46\ M_\odot$ at a distance of 500 pc. This mass can be considered as a lower limit since it is not corrected for H I absorption. On the other hand, if we integrate the absorption-corrected spectrum (dashed line in Fig. 2), the H I column density is $N_{HI} \sim 1.7\times10^{21}$ cm^{-2} and the H I mass is $M_{HI} \sim 1.2\ M_\odot$. The N_{HI} obtained from the absorption-corrected spectrum compares very well with the value ($N_{HI} \sim 1.4\times10^{21}$ cm^{-2}) predicted by van Dishoeck & Black's (1988) model for NGC 2023, while the N_{HI} from the observed uncorrected spectrum is a factor of $\sim$ 2.5 lower than the predicted value.

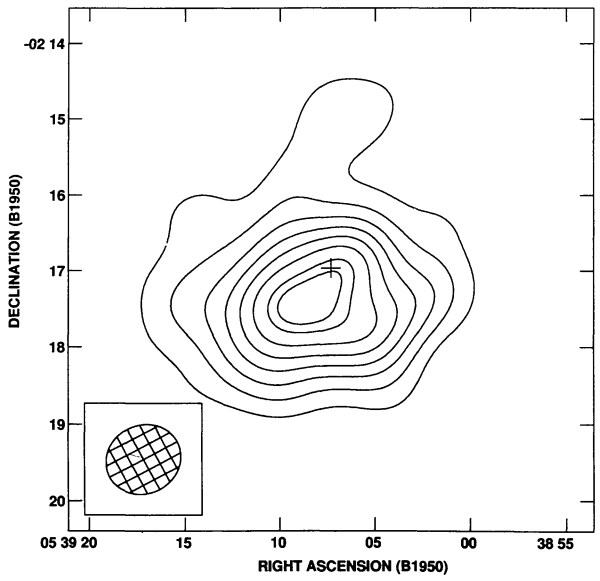

Figure 3. Map of integrated 21 cm emission from 5.1 to 14.2 km s^{-1}. Contour levels are -4, 4, 6, 8, 10, 12, 14, 16, 17 times 10 mJy beam^{-1}. The cross indicates the position of HD 37903, and the beam is shown in the bottom left corner.

A map of the integrated H I emission is shown in Figure 3. The peak emission is clearly not at the stellar position, but rather is shifted $\sim$ 30″ to the southeast. This shift can be explained in term of the geometry proposed by Draine & Bertoldi (1996), where the bulk of the cloud is displaced to the south of HD 37903.

3.3. Comparison with Other Observations

In the reflection nebula NGC 7023 Rogers et al. (1995) found that the H I line emission coincides with the FIR dust emission. To determine if a similar coincidence occurs for NGC 2023, we compare in Figure 4 our 21 cm flux density map with the HIRES 60 μm map processed by IPAC[2], and the [C II] (158 μm) map of Howe et al. (1991). In Figure 4 we also present a contour map of a digitized POSS image (Klinglesmith & Hollis 1987). We convolved the optical image with a gaussian beam of 50″$\times$ 50″ in order to obtain a similar resolution to that of the H I map. We see that the general shape of the H I line emission is similar to the C II line emission, to the 60 μm continuum emission, and the POSS contour map. A feature that we wish to emphasize is that the maximum of the emission in each contour map is offset $\sim$ 30″ from the position of HD 37903: to the south (in the 60 μm map), and the southeast (in the C II and H I maps). The similarities between these maps suggest that the emitting region could be the same in all of them. Steiman-Cameron et al. (1997) applied a two-phase model to NGC 2023 to reproduce the observed intensities of the far IR fine structure lines of [O I] and [C II]. One of the component of the model is compact and has high temperature (T $\sim$ 700 K) and density (n $\sim 10^5$ cm^{-3}), while the other is more extended and has T $\sim$ 260 K and n $\sim$ 750 cm^{-3}. They argue that the C II emission comes from both compo-

[2] The Infrared Processing Analysis Center (IPAC) was established as the National Aeronautics and Space Administration (NASA) archival center for the *Infrared Astronomical Satellite (IRAS)* data. IPAC is operated by the Jet Propulsion Laboratory (JPL) and California Institute of Technology (Caltech) for NASA. IPAC was founded by NASA as part of the IRAS extended mission program under contract to JPL/Caltech.

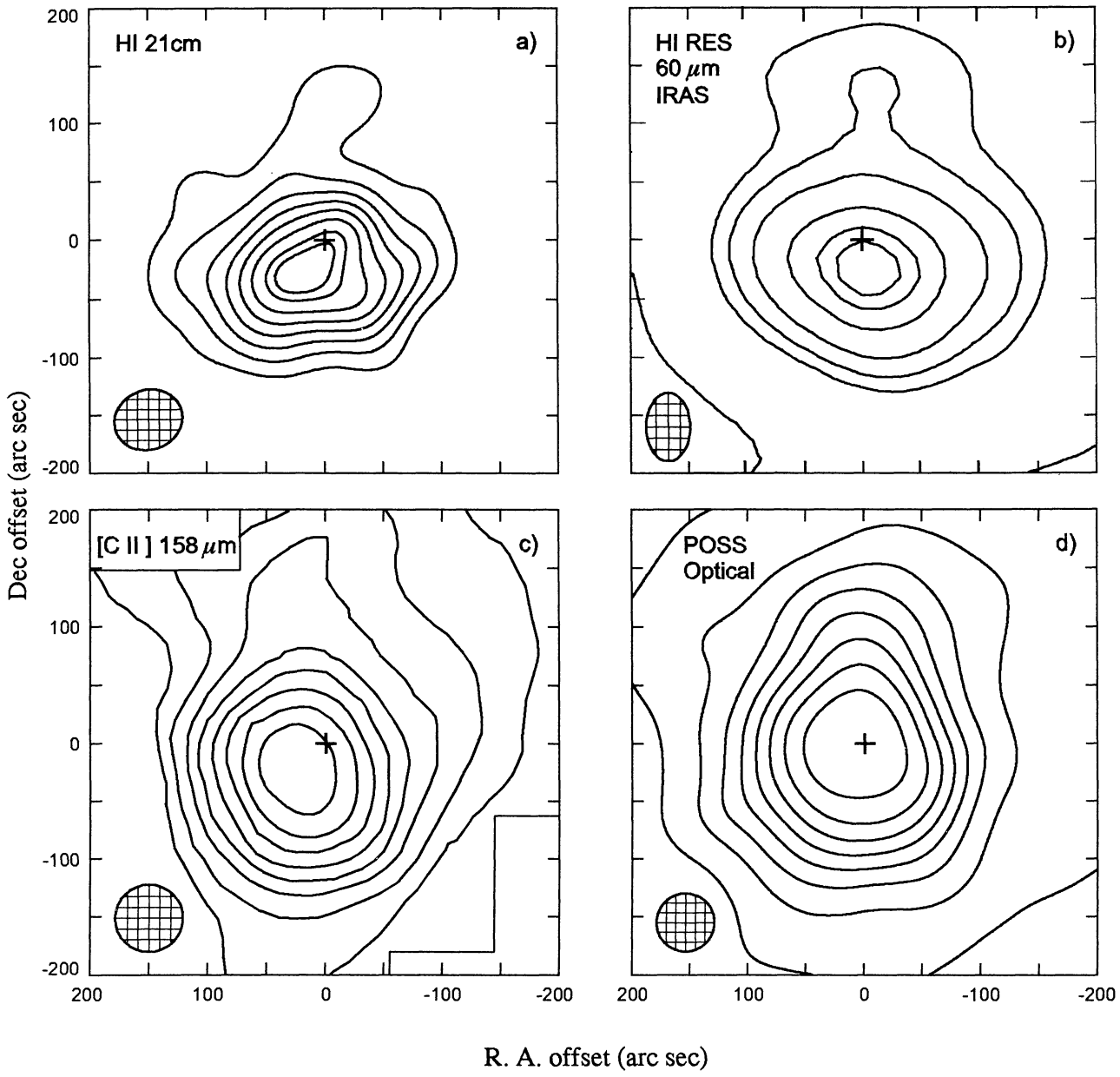

Fig. 4. a) 21 cm H I integrated map. Contours are the same as in Figure 3. b) 60 μm HIgh RESolution IRAS surface brightness map, with contours of -5, 5, 40, 60, 100, 200, 300, 370 times 19.73 MJy sr^{-1}. The FWHM of the effective *IRAS* beam after 20 iterations is $68'' \times 44''$ (similar to the VLA beam) and it is shown in the map. c) 158 μm [C II] map taken from Howe et al. (1991) with contours of 0.2, 0.3, 0.4, 0.5,0.6, 0.7, 0.8, 0.9 times 9.01×10^{-4} erg s^{-1}cm^{-2}sr^{-1} with a $55''$ beam. d) POSS contour map. The image was convolved with a $50'' \times 50''$ gaussian beam in order to obtain a similar resolution to that of the H I map. The contours levels are 0.2, 0.3, 0.4, 0.5,0.6, 0.7, 0.8, 0.9 times the peak value of the map. The position (0,0) in each map corresponds to HD 37903 and is indicated by the cross.

nents and the O I emission comes from the compact component. We believe that the 21 cm H I line emission could come from the same extended region as the C II region seen in the 158 μm line. Photodissociation models predict that the H I region coexists with the C II region but the penetration of the C II region into the molecular cloud is deeper than that of the H I region (e.g., Jaffe & Howe 1989; Hollenbach 1990; Roger & Dewdney 1992). The similarities between the maps suggest that the extension of the C II region into the cloud is not very different to that of the H I.

3.4. An Independent Photodissociated Region in NGC 2023?

In Figure 1 we noted the presence of a local H I peak to the north of HD 37903. This emission is only present in the 12.9 and 11.6 km s^{-1} channels. This local peak of H I emission could be also photodissociated by HD 37903, or could correspond to a region excited by an independent star embedded $\sim 2'$ north of HD 37903. If we assume the existence of an embedded star we can estimate its spectral type based on the H I emission (Rodríguez et al. 1990). We obtain an H I column density of $\sim 2\times10^{20}$ cm^{-2} and an H I mass of 0.029 $M_\odot$ (distance = 500 pc), assuming optically thin emission. We used a source size of $53''\times59''$ which is an upper limit to the size because the emission is not resolved. This column density and mass are lower limits because of the optically thin assumption. Using this mass and size, we can estimate the rate of photodissociating far UV radiation from the equation

$$\frac{\dot{N}}{10^{30}s^{-1}Hz^{-1}} = 0.73\left(\frac{M_{HI}}{0.01M_\odot}\right)^2\left(\frac{R}{0.01pc}\right)^{-3}$$

$$exp\left[4.7\left(\frac{M_{HI}}{0.01M_\odot}\right)\left(\frac{R}{0.01pc}\right)^{-2}\right] ,$$

taken from Rodríguez et al. (1990). The rate of photodissociated far UV radiation is found to be $\dot{N} = 2.6\times10^{28}$ s^{-1} at λ =1000 A. This rate corresponds to a main sequence star of spectral type B9. The source IRAS 0539−0214 is near the position of the northern H I emission peak. From Figure 4, we note that the local maximum to the north of HD 37903 is also detected clearly in the HIRES 60 μm *IRAS* map, and it is also evident in the [C II] and optical maps (see Fig. 4). The fact that the secondary peak appears also in the optical image favors the interpretation that it is being photodissociated by HD 37903. Further research is needed to establish the nature of this secondary peak to the north of HD 37903.

4. CONCLUSIONS

We detected compact H I line emission in NGC 2023. The spectrum appears to be absorbed by a neutral foreground medium. The H I column density determined by using the absorption-corrected spectrum was $\sim 1.7\times10^{21}$ cm^{-2} with an H I mass of $\sim 1.2M_\odot$ at a distance of 500 pc. The observed column density agrees well with the theoretical model of van Dishoeck & Black (1988). From comparisons of the H I maps with the FIR continuum emission from warm dust (at 60 μm), POSS contour map and [C II] (at 158 μm) we note a strong similarity between all maps. We suggest that the H I emission may be coming from the same extended region that produces the [C II] infrared emission.

ML and LFR acknowledge support from DGAPA, UNAM and from PADEP, UNAM.

REFERENCES

Crawford, M. K., Genzel, R., Townes, C. H., & Watson, D. M. 1985, ApJ, 291, 755
Dewdney, P. E., Roger, R. S., Purton, C. R., & McCutcheon, W. H. 1991, ApJ, 370, 243
Draine, B. T., & Bertoldi, F. 1996, ApJ, 468, 269
Gómez, Y., Lebrón, M. E., Rodríguez, L. F., Garay, G., Lizano, S., Escalante, V. & Cantó, J. 1997, in preparation
Hollenbach, D. J. 1990, in ASP Conf. Ser. Vol. 12, The Evolution of the Interstellar Medium, ed. L. Blitz, (San Francisco: ASP), 167
Howe, J. E., Jaffe, D. T., Genzel, R., & Stacey, G. J. 1991, ApJ, 373, 158
Jaffe, D. T., & Howe, J. E. 1989, RevMexAA, 18, 55
Jaffe, D. T., Genzel, R., Harris, A. I., Howe, J. E., Stacey, G. J., & Stutzki, J. 1990, ApJ, 353, 193
Klinglesmith, D. A., & Hollis, J. M. 1987, ApJS, 64, 127
Knapp, G. R., Brown, R. L., & Kuiper, T. B. H. 1975, ApJ, 196, 167
Kramer, C., Stutzki, J., & Winnewisser, G. 1996, A&A, 307, 915
Lada, E. A., Bally, J., & Stark, A. A. 1991, ApJ, 368, 432
Launhardt, R., Mezger, P. G., Haslam, C. G. T., Kreysa, E., Lemke, R., Sievers, A., & Zylka, R. 1996, A&A, 312, 569
Levinson, F. H., & Brown, R. L. 1980, ApJ, 242, 416
Moriarty-Schieven, G. H., Xie, T., & Patel, N. A. 1996, ApJ, 463, L105
Pankonin, V., & Walmsley, C. M. 1976, A&A, 48, 341
_____. 1978, A&A, 67, 129
Rodríguez, L. F., Lizano, S., Cantó, J., Escalante, V., & Mirabel, I. F. 1990, ApJ, 365, 261
Roger, R. S., & Dewdney, P. E. 1992, ApJ, 385, 536
Roger, R. S., & Leahy, D. A. 1993, AJ, 106, 31
Rogers, C., Heyer, M. H., & Dewdney, P. E. 1995, ApJ, 442, 694
Sellgren, K. 1983, AJ, 88, 985
Sellgren, K., Werner, M. W., & Dinerstein, H. L. 1992, ApJ, 400, 238
Steiman-Cameron, T., Hass, M. R., Tielens, A.G.G.M., & Burton, M. G. 1997, ApJ, 478, 261
van Dishoeck, E. F., & Black, J. H. 1988, ApJ, 334, 771
Wyrowski, F., Walmsley, C. M., Natta, A., & Tielens, A.G.G.M. 1997, A&A, 324, 1135

Mayra Lebrón and Luis F. Rodríguez: Instituto de Astronomía, UNAM, Apartado Postal 70-264, 04510 México, D.F., México. (mlebron, luisfr@astrosmo.unam.mx).